# Spatial reconstruction of events in a Compton telescope

Jessie Thwaites

23 April 2021

**Abstract**

This project aims to simulate events from the Crab Nebula seen in the COMPTEL space-based Compton telescope, and reconstruct them following the methods described in Boggs and Jean [2000]. Reconstructions are performed using a toy Monte Carlo method, and probability density functions for the incoming energy and scattering angle are used to generate the data. Reconstructions of events consisting of between 7-10 photons interacting in the detector are presented. 1,000 of these events are simulated to investigate the consistency of the results and the trial variation, and are shown to be accurate to the true source location within error for 99.8% of reconstructions. Using a toy Monte Carlo method, the position of the Crab Nebula is reconstructed to $83.61 \pm 0.12$ degrees in right ascension and $21.98 \pm 0.14$ degrees in declination, which is within uncertainty for the actual source location.

## 1    Introduction

Compton scattering happens when a photon elastically scatters off an electron, and this process dominates the photon total cross section in the keV-MeV range [Tavernier, 2010]. Many interesting sources can be studied in this energy range, including active galactic nuclei, supernova remnants, the Sun during flares, and many others [Schoenfelder and the COMPTEL Collaboration, 2000].

The necessity of capturing photon data in this energy range prompted the development of space-based Compton telescopes. One of the earliest Compton telescopes was COMPTEL, which was launched aboard the Compton Gamma-ray Observatory in 1991, and collected data until 2000. A schematic of COMPTEL can be seen in Figure 1. It performed the first all-sky survey in the energy range 1-30 MeV [Boggs and Jean, 2000].

In a Compton telescope, direction and energy information from two or more Compton interactions in the detector with photons from a single source allows the reconstruction of the source location and direction. A detailed description of the COMPTEL detector can be found in Schönfelder et al. [1993], and a catalogue of sources found by COMPTEL can be found in Schoenfelder and the COMPTEL Collaboration [2000].

## 2    Principles of Compton telescope imaging

This section will follow closely the reconstruction methods for events in Compton telescopes outlined in Boggs and Jean [2000].

A Compton telescope is generally made up of two or more layers of scintillator material. In a telescope with two layers of scintillator the incoming photon undergoes a Compton scatter in

| D1 total area | D2 total area | Energy range | Field of view | Angular res. | Energy res. |
|---|---|---|---|---|---|
| 4300 cm$^2$ | 8600 cm$^2$ | 0.8-30 MeV | 1 sr | 1.7-4.4$^o$ | 5-8% FWHM |

Table 1: Specifications for COMPTEL, from Schönfelder and Kanbach [2013]. D1 and D2 are modules of scintillator in the upper and lower detectors, respectively.
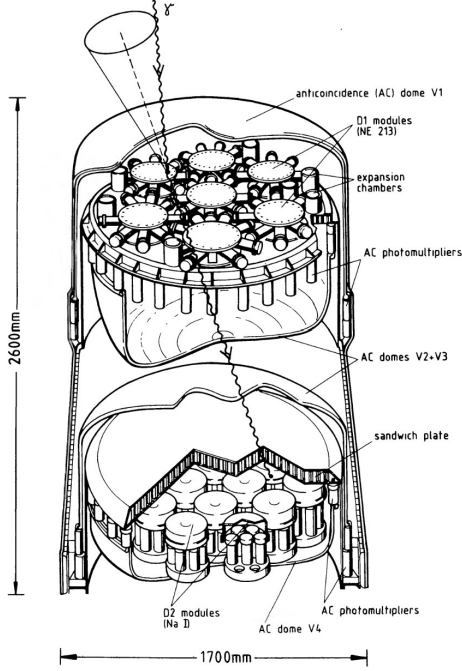


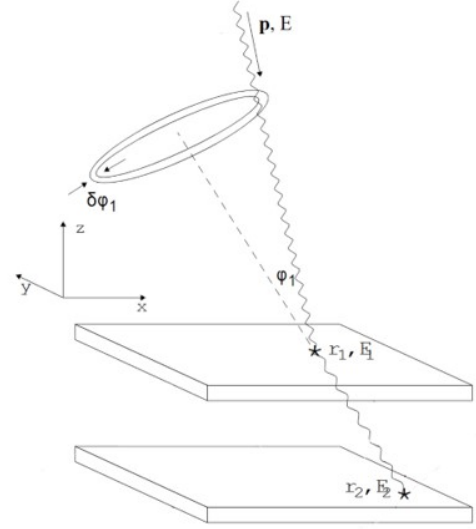Figure 1: Schematic drawing of COMPTEL, from Schönfelder et al. [1993].



Figure 2: A scatter event for a photon with energy E and momentum $\vec{p}$ inside the Compton telescope. Adapted from Boggs and Jean [2000]

.

the low-Z scintillator in the top plane of the detector and undergoes a photoelectric absorption interaction in the high-Z scintillator of the lower plane of the detector.

A schematic of COMPTEL can be seen in Figure 1. COMPTEL has two planes of scintillator modules (D1 in the upper detector and D2 in the lower detector). Some specifications for COMPTEL can be seen in Table 1.

As is shown on Fig. 2, an incoming photon of energy $E$ and momentum $\vec{p}$ scatters in the first layer of the detector at position $\vec{r_1}$, depositing energy $E_1$ in the form of a recoil electron. It is absorbed at the point $\vec{r_2}$, depositing its remaining energy $E_2$, which is given by [Tavernier, 2010]:

$$E_2 = \frac{E}{1 + \frac{E}{m_e c^2}(1 - \cos\phi)} \tag{1}$$

Then the scatter direction is $\vec{r_1'} = \vec{r_2} - \vec{r_1}$, and the reconstruction angle is given by:

$$\hat{r_1}' \cdot \hat{p} = \cos\phi_1 = 1 + \frac{1}{W_0} - \frac{1}{W_1} \tag{2}$$

2

Where $W_0$, $W_1$ are the total energy and energy after the scatter, normalized to the electron mass, such that

$$W_0 = \frac{E}{m_e c^2} = \frac{E_1 + E_2}{m_e c^2}$$

$$W_1 = \frac{E_2}{m_e c^2} \tag{3}$$

This initial direction $\hat{p}$ is not unique, as this reconstruction does not give azimuthal information, so Equation 2 only gives a cone of directions, which can be projected as a circle on the sky.

The uncertainty of this reconstructed cone is dependent on the energy uncertainty of the telescope. For COMPTEL, the energy uncertainty ranges from 5-8.8% FWHM [Schönfelder and Kanbach, 2013]. In this reconstruction, the more conservative end of this range (8.8% FWHM) is selected, which is related to the 1-$\sigma$ errors plotted as $\delta = \sigma_{FWHM}/2\sqrt{2\ln2}$, where $\delta$ is the percent error at 1-$\sigma$. Then, the angular uncertainty of our reconstruction takes the form:

$$\delta\phi_E = \frac{1}{\sin\phi} \left[ \left( \frac{\delta^2}{W_0^2} \right) + (\delta W_1)^2 \left( \left( \frac{1}{W_1^2} - \frac{1}{W_0^2} \right)^2 - \frac{1}{W_0^4} \right) \right]^{1/2} \tag{4}$$

This reconstruction gives a set of cones at angles of $\phi_1$ with the $\hat{r_1}'$ axis, with a width corresponding to the angular uncertainty $\delta\phi_E$.

# 3 Reconstruction Methods

This reconstruction will focus on simulating data from the Crab Nebula in the COMPTEL telescope. Section 3.1 describes the method for simulating data in the detector using a monoenergetic source incident from directly above the detector. Using this energy, a probabilty distribution function can be drawn for the scattering angle of the photon after the interaction, and simulate a number of events in the telescope. From here, Section 3.2 will describe the reconstruction of the source location using the conical projections described by Equation 2 and a toy Monte Carlo method.

## 3.1 Simulating COMPTEL detector data

For given incoming photon energy, there is a probability density function for the scattering angle of the Compton scatter in the first layer of the detector, which is given by the differential cross section:

$$\frac{d\sigma}{d\Omega} = \left( \frac{r_0^2}{2} \right) \left( \frac{E_2}{E} \right)^2 \left( \frac{E_2}{E} + \frac{E_2}{E} - \sin^2\theta \right) \tag{5}$$

With $E_2$ as the final energy deposited in the detector, and $E$ the total initial photon energy (as shown in Fig. 2). The normalized PDFs for three sample values for the initial energy can be seen in Figure 3a. For a given energy, the angle can be chosen according to this PDF, which can then be used with Equation 1 to get a value for the energy after the scatter. These final energies can be seen in 3b, which was drawn by 10,000 random samples of the angular PDF for that corresponding initial energy.

The simulation is written in Python and uses a toy Monte Carlo method for reconstructing photons in the detector. The simulation starts by assuming a source incident on the detector from directly above. It then chooses a scattering angle from the angular PDF given an initial energy
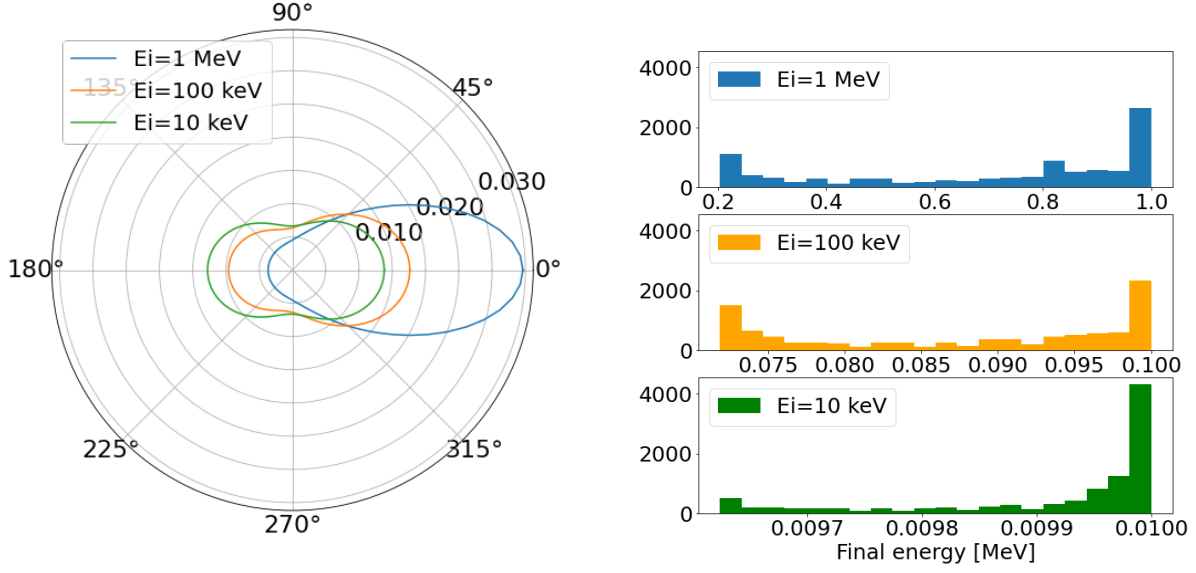
(a) Normalized angular PDF for Compton scatters, at various initial energies.

(b) Monte Carlo realizations of final energies for selected initial energies, with random draws of scattering angle according to angular PDF in 3a.

Figure 3: Distributions used to create events in the detector, according to Equations 1 and 5.
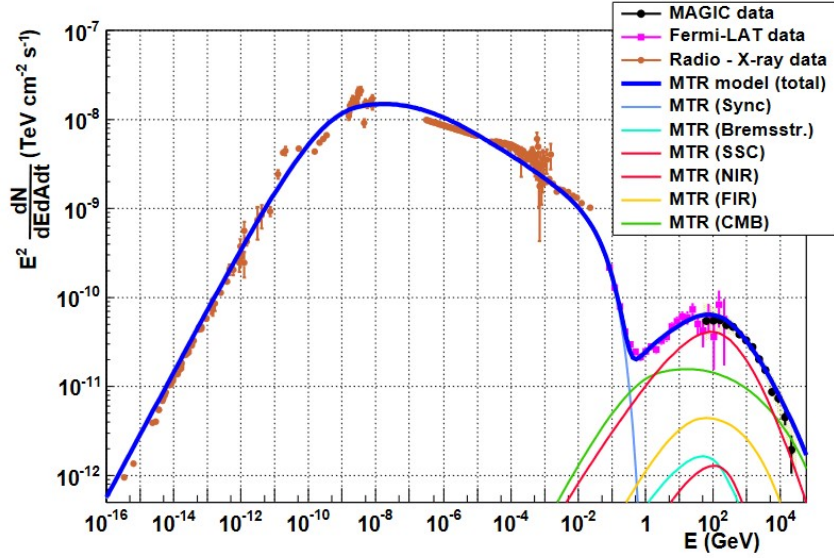


Figure 4: High precision measurements of the full spectrum of the Crab, from MAGIC Collaboration [2015].

and calculates the final energy for the scatter. To simulate position data in the detector, a point on the upper detector, $\vec{r_1}$, and an axis for the scatter, $\hat{r_1}'$, are chosen. The photon is propagated along the $\hat{r_1}'$ direction to the point $\vec{r_2}$ in the lower detector. The simulated location is then shifted to the source location on the sky.

## 3.2   Reconstructions of the Crab Nebula

The Crab Nebula is a bright source often used as a calibration source due to its high luminosity. Because of this, it has been precisely measured across many wavelengths, and its full spectrum can be seen in Figure 4 [MAGIC Collaboration, 2015]. Starting with the simulated events described in the last section, the code projects the reconstructed cone of directions as a circle onto the sky, and calculates a 1-$\sigma$ uncertainty according to Equation 4.

The source location can be reconstructed by creating a 2-D histogram through a toy Monte Carlo method. The $1 - \sigma$ angular uncertainty for each reconstruction (calculated in Eqn. 4) is assumed to be normally distributed. For each point in the circular reconstruction, 1000 points are randomly drawn from a normal distribution with the point as the mean and $\delta\phi_E$ the standard deviation of the distribution. Using this method allows us to distribute the errors along the curve to effectively weight the error distribution for each photon reconstruction. All of these points for each photon in the event (here, 7-10 photons are used per event) are collected, and are used to construct a 2-D histogram of all of the reconstructions and their errors. Two of these 2D histograms can be seen in Figure 5.

These can be seen to accurately reconstruct the Crab location within the reported $1 - \sigma$ uncertainties (true location of the Crab is $86.63^o$ in right ascension (RA) and $22.01^o$ in declination). However, it can also be seen that this method weights the photons which are reconstructed with smaller radii more heavily (and these thus appear brighter on Fig. 5). There is no physical reason that these should be more heavily weighted, but is a consequence of using this method for determining the reconstruction location. This may contributed to the fact that the errors on the reconstruction directions appear very small, instead of the $1.7 - 4.4^o$ angular resolution expected from Schönfelder and Kanbach [2013] shown in Table 1.

At first, for simplicity and testing of the code, the source is approximated as monoenergetic, or a delta function in energy. A set of four sample reconstructions at different single values of energy can be seen in Figure 6. However, a delta function in energy is not a physically accurate description of the source. A more physical representation would be allowing the simulation to draw from a continuum of energies produced by the source, weighted according to the fluxes for those particular energies. The portion of the full Crab spectrum (Fig. 4) in the the energy range that COMPTEL covers (Table 1) is isolated and normalized for use as a probability distribution. The Monte Carlo method can then draw values from this normalized spectrum, shown in Fig. 7.

The event simulation source location is done as described in the previous section using the same toy Monte Carlo method, but each photon in the event has an energy drawn from this spectrum. Four sample reconstructions using this method can be seen in Figure 8.

(a) Reconstruction location:
RA: $83.62 \pm 0.10^o$, Declination: $22.01 \pm 0.08^o$

(b) Reconstruction location:
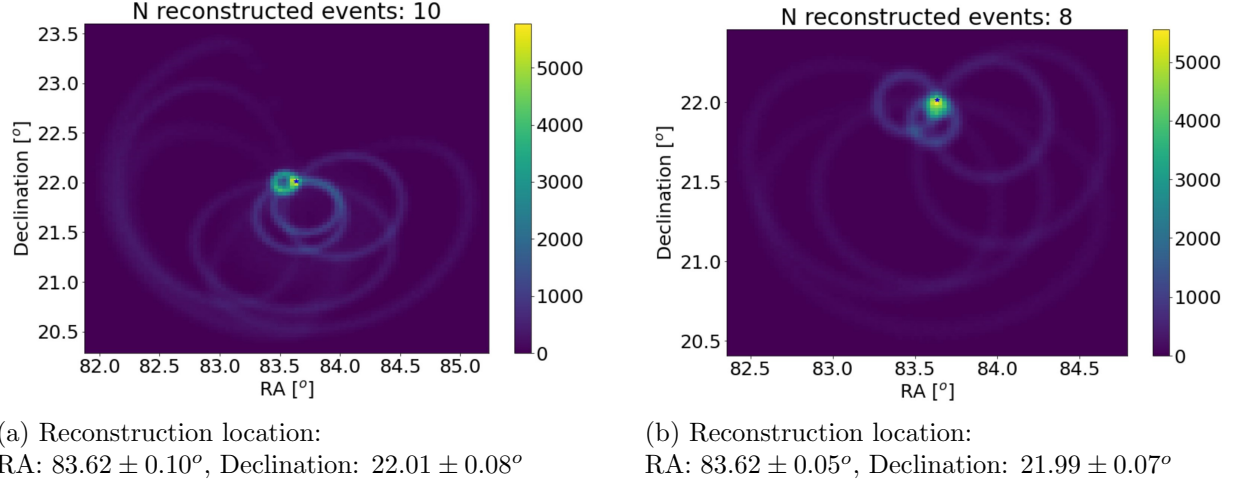RA: $83.62 \pm 0.05^o$, Declination: $21.99 \pm 0.07^o$

Figure 5: Two sample 2-D histogram reconstructions of circular reconstruction projections from toy Monte Carlo method. Colors indicate number of points in each bin. Values indicate bin with highest value, which is used as the reconstruction location, and errors indicate bins with values greater than 1/2 of the maximum value in the bin.
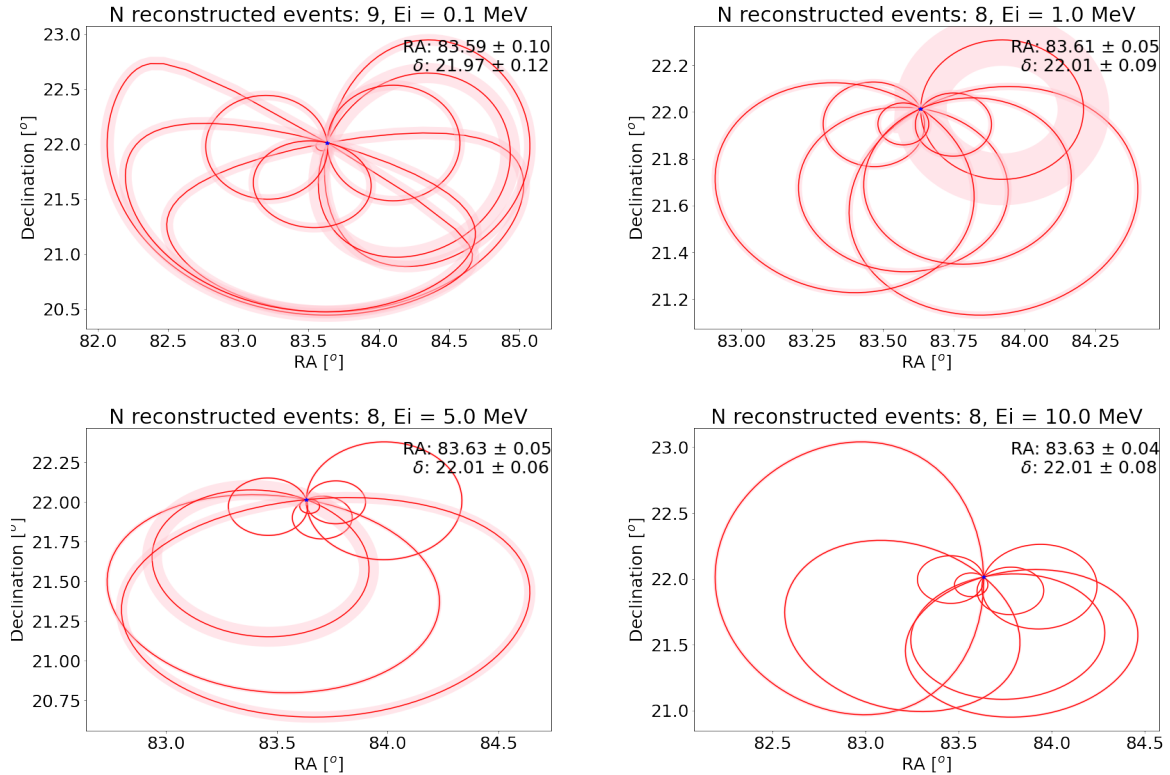


Figure 6: Reconstructions with a delta function energy PDF, with angular errors. Cones projected onto the sky are drawn as red circles, and the location of the Crab Nebula is plotted as a blue star in the center.
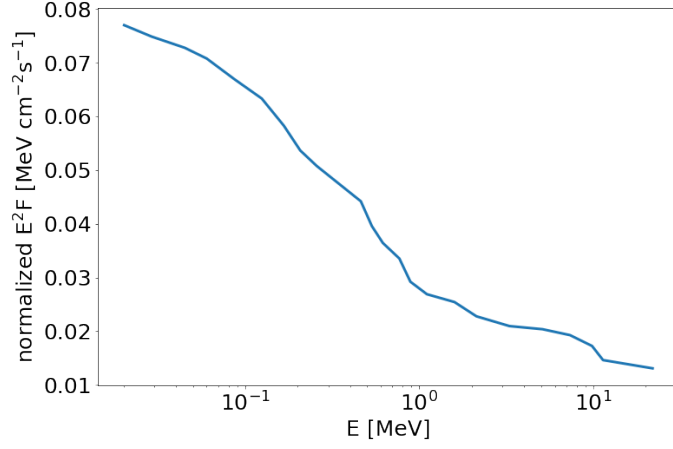
Figure 7: The 0.02-30 MeV portion of the Crab spectrum, using digitized data from Fig. 4. Normalized for use as a PDF of incoming photons to the detector.
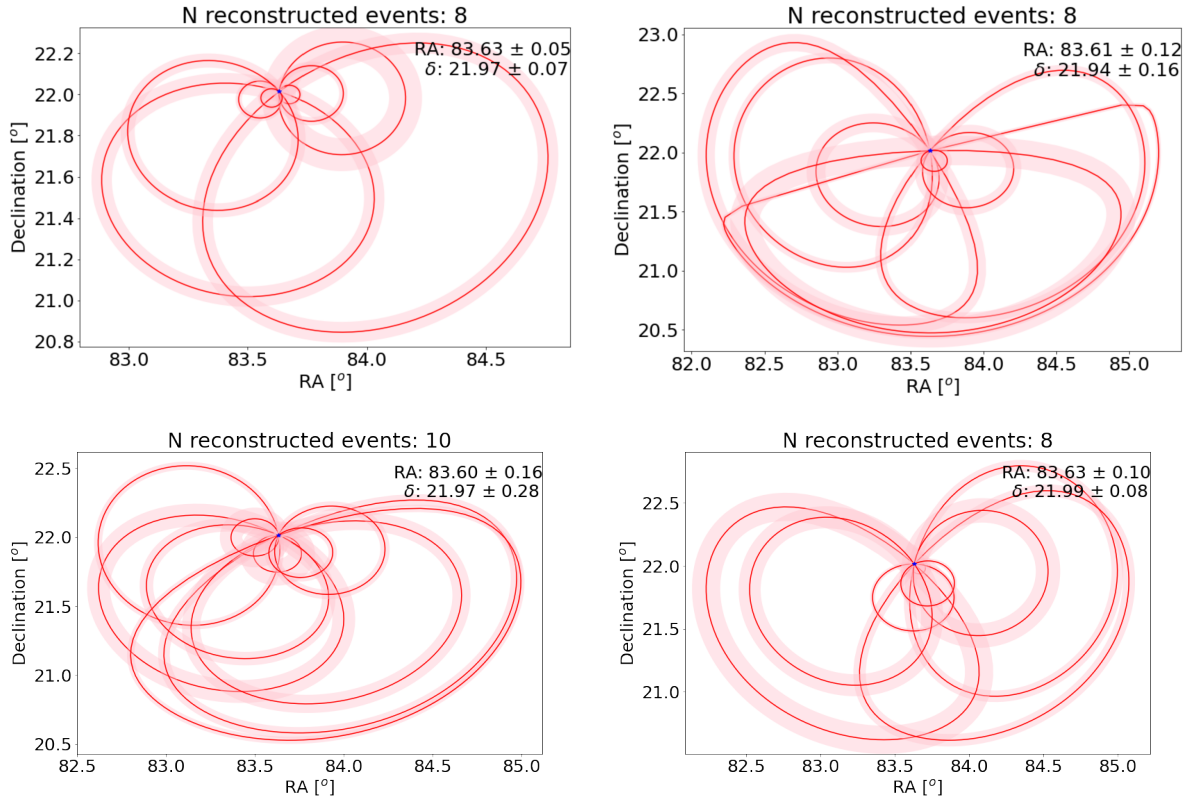


Figure 8: Reconstructions made by drawing energy values from the energy PDF for the Crab Nebula shown in Figure 7.
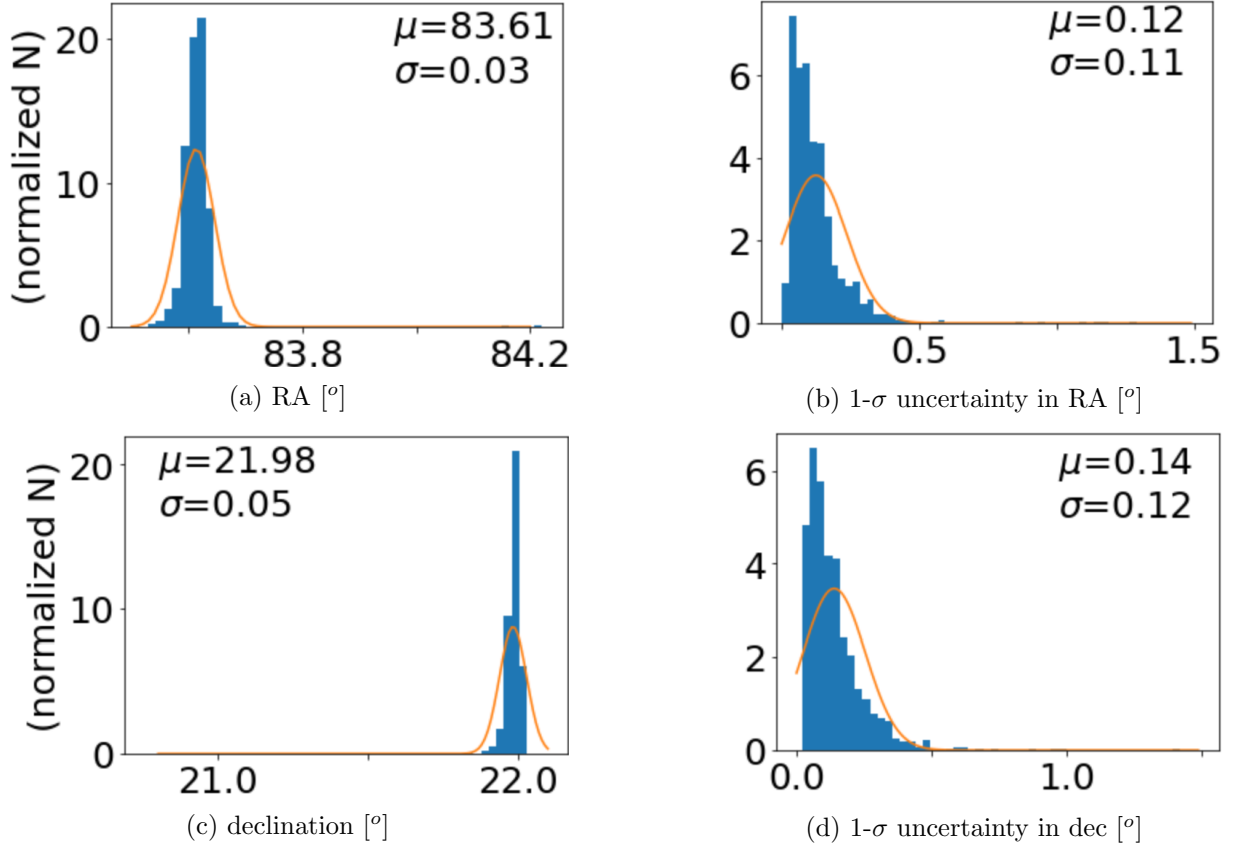
Figure 9: Histograms of reconstructed source right ascension and declination values for 1,000 Crab Nebula events. Each event is 10 photons interacting in the detector. Orange lines show Gaussian fits, and fit parameters ($\mu$ as the mean and $\sigma$ the standard deviation) are displayed on the plot.

# 4    Reconstruction results and trial variation

Since each reconstruction has a limited number of photons interacting within the detector, it was important to investigate the precision and repeatability of our results. For this a toy Monte Carlo method with 1,000 trials was used to reconstruct events with 7-10 photons in the detector. All of these histograms are fitted with a Gaussian function, with the assumption that variation in these parameters are statistical fluctuations. The histograms are normalized in order to compare with the Gaussian fits. All of these histograms and fits can be seen in Figure 9. The first column (Figs 9a and 9c) are the histograms for RA and declination, respectively, and the second column (Figs 9b and 9d) are histograms of the errors reported on the values.

From the shape of the fits it appears that none of these histograms follow a Gaussian shape well. (A chi-squared value was also computed, and with a very high chi-squared value and low p-value, these showed that the histograms are not well fit by their Gaussian fits.) For the RA and declination histograms (Figs 9b and 9d), this could be due to an underestimation of the errors on the reconstruction location, as described in Section 3.2. There are also some outlying points on the RA and declination histograms that are much greater than $3 - \sigma$ away from the mean (for RA, two points with RA greater than $84^o$, and for declination one point with declination less than $21^o$).

8

These points are well outside the statistically expected range expected in these reconstructions. However, it should be noted that these points are still within the error reported by COMPTEL (Table 1, Schönfelder and Kanbach [2013]).

For the uncertainty histograms (Figs 9b and 9d), this could be because the histograms are peaked near 0, and thus show a single-tailed distribution shape. However, the fits give a good estimate for the mean error and its spread. There is no physical reason that the angular uncertainty should differ between the RA and declination distributions, and our values do not show a significant difference in these. However, these do appear to be an order of magnitude different than those expected from Schönfelder and Kanbach [2013] (Table 1).

# 5    Conclusions

The goal of this project was to simulate Compton interaction events in the COMPTEL detector, using the Crab Nebula as a source, and to reconstruct these events using a toy Monte Carlo method. Using this method with events consisting of between 7-10 photons interacting in the detector, the location of the Crab can be reconstructed to within our 1-$\sigma$ uncertainty.

The consistency and reproducability of these results was also tested, and for 99.8% of the trials with this number of photons the reconstruction produced accurate results. The location for the Crab Nebula is reconstructed via this Monte Carlo method to $83.61 \pm 0.12^o$ RA and $21.98 \pm 0.14^o$ declination, which is within uncertainty of the true value ($86.63^o$ in RA and $22.01^o$ in declination).

The uncertainties on these reconstructions were approximately an order of magnitude smaller than expected, with a mean 1-$\sigma$ uncertainty of $0.12^o$ in RA and $0.14^o$ in declination rather than the $1.7 - 4.4^o$ expected (Table 1, Schönfelder and Kanbach [2013]). There are several reasons that this could be the case. One possibility, as discussed previously in Section 3.2, was the disproportionate weighting of the reconstructions based on the radius of the projection drawn. This does not have a physical interpretation, but is rather due to the method of weighting the uncertainties on the values of the reconstructions in the toy Monte Carlo.

Another possibility is the number of photons interacting in the detector in a single event. A reconstructed direction cannot be determined for a single photon event, but requires two or more photons undergoing Compton scattering in the telescope. In this paper, each event had between 7-10 photons interacting in the telescope. This number was chosen in order to get a better distribution of values from both the energy PDF and scattering angle PDF. However, this is more photons than would necessarily be required to resolve an event (the minimum being two photons). As the number of photons interacting in the detector increases, the uncertainty of the final source location reconstruction decreases. Thus, if the average number of photons considered as an event for COMPTEL is lower than this work, this could also explain some of the difference in energy resolution found in this work.

This work also did not consider time coincidence of photons in the telescope, or rate of photons incident on the detector. Here, we used the flux measurements for the Crab to create a spectrum of energies for photons, but it would also be interesting to integrate these fluxes over a particular time window to find an average number of photons that would interact in the detector in a given time window. However, this discussion would also require analysis of background events from other sources incident on the telescope as well, and perhaps also information about coincidence of photons to more accurately reconstruct the events in the detector. This analysis of time dependency is outside the scope of this work, but would give insight for the true number of photons that

should be simulated for each event, and thus change the uncertainty on the final source location reconstruction.

## 6 Code

The GitHub repository for this project can be found at `github.com/jessiethw/COMPTEL-project`.

## References

S. E. Boggs and P. Jean. Event reconstruction in high resolution Compton telescopes. *Astron. Astrophys. Suppl. Ser.*, 145(2):311–321, Aug. 2000. ISSN 0365-0138, 1286-4846. doi: 10.1051/aas: 2000107.

MAGIC Collaboration. Measurement of the Crab Nebula spectrum over three decades in energy with the MAGIC telescopes. *Journal of High Energy Astrophysics*, 5-6:30–38, Mar. 2015. ISSN 22144048. doi: 10.1016/j.jheap.2015.01.002. URL `http://arxiv.org/abs/1406.6892`.

V. Schoenfelder and the COMPTEL Collaboration. The first COMPTEL Source Catalogue. Feb. 2000. doi: 10.1051/aas:2000101. URL `http://arxiv.org/abs/astro-ph/0002366`.

V. Schönfelder and G. Kanbach. Imaging through Compton scattering and pair creation. In M. C. E. Huber, A. Pauluhn, J. L. Culhane, J. G. Timothy, K. Wilhelm, and A. Zehnder, editors, *Observing Photons in Space*, pages 225–242. Springer New York, New York, NY, 2013. ISBN 978-1-4614-7803-4 978-1-4614-7804-1. doi: 10.1007/978-1-4614-7804-1\_11.

V. Schönfelder, H. Aarts, K. Bennett, H. de Boer, J. Clear, W. Collmar, A. Connors, A. Deerenberg, R. Diehl, J. Macri, M. McConnell, D. Morris, R. Much, J. Ryan, G. Simpson, M. Snelling, G. Stacy, H. Steinle, A. Strong, B. N. Swanenburg, B. Taylor, C. de Vries, and C. Winkler. Instrument description and performance of the imaging gamma-ray telescope COMPTEL aboard the Compton gamma-ray observatory. 86(2):36, june 1993. doi: 10.1086/191794. URL `http://articles.adsabs.harvard.edu/pdf/1993ApJS...86..657S`.

S. Tavernier. *Experimental Techniques in Nuclear and Particle Physics*. Springer-Verlag, Berlin Heidelberg, 2010. ISBN 978-3-642-00828-3. doi: 10.1007/978-3-642-00829-0.